UNIVERSITAT POLITÈCNICA DE CATALUNYA

GEOPLEX: Benchmark Demonstration

C. Batlle, A. Dòria, E. Fossas

Institut d'Organització i Control de Sistemes Industrials

Geoplex Benchmark Demonstration.

C. Batlle[1,2,4], A. Dòria[4] and E. Fossas[3,4]
[1]EPSEVG, [2]MAIV, [3]ESAII, and [5]IOC
Technical University of Catalonia

October, 2003

1 Electromechanical benchmark

In this section, we describe the development of a complex multi-domain electromechanical system as an interconnection of simpler subsystems. We first give a global overview of the total system to be modelled, then describe the subsystems of the model, and conclude with final remarks on how network modelling was used in this problem, and to what benefit.

Our electromechanical system exchanges energy between the power grid, a local mechanical source and a local general load, which may contain subsystems from any domain.

1.1 System overview

A general description of our system appears in Figure 1.

The core of our model is a doubly-fed induction machine (DFIM) together with its controller, a back-to-back 3phase converter (B2B). The DFIM is coupled to the power grid directly through the stator, while the rotor receives power from the B2B, which in turn takes it from the power grid.

The control objective, which does not form part of this Deliverable, is to effect the flow of power from the grid and the local source to the local load, by means of Hamiltonian and port related ideas.

The `20sim` model of the whole system, in bond graph notation, appears in Figure 2. We have suppressed the transformers and the dynamics of the flywheel's beam, but they can be incorporated easily from the `20sim` library.

We will describe the DFIM with some detail since it is the most complex of the subsystems and the one with more room for modelling improvement.

1.2 The doubly-fed induction machine

The doubly fed induction machine appears in Figure 1.2

It contains 6 energy storage elements with their associated dissipations and 6 inputs (the 3 stator and the 3 rotor voltages). The dynamical equations are ([8][10], but see [4][2] for a discussion)

$$v = Ri + \frac{\mathrm{d}\lambda}{\mathrm{d}t} \tag{1}$$

where $R = \mathrm{diag}(r_s, r_s, r_s, r_r, r_r, r_r)$ and the linking fluxes are related to the currents through an angle-dependent inductance matrix

$$\lambda = \tilde{L}(\theta)i. \tag{2}$$

We assume that

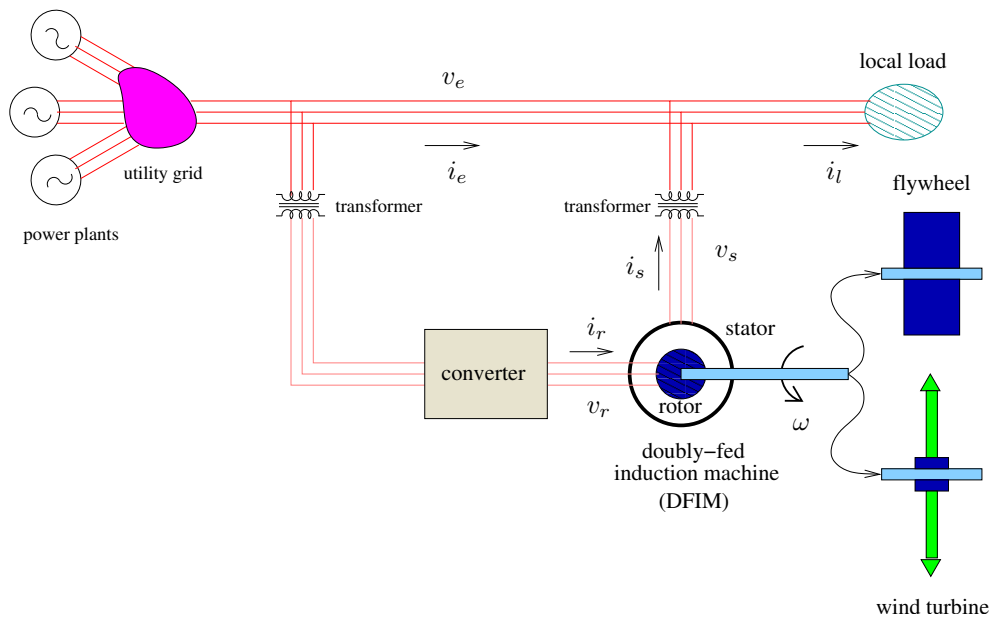- the machine is symmetric (all windings are equal)
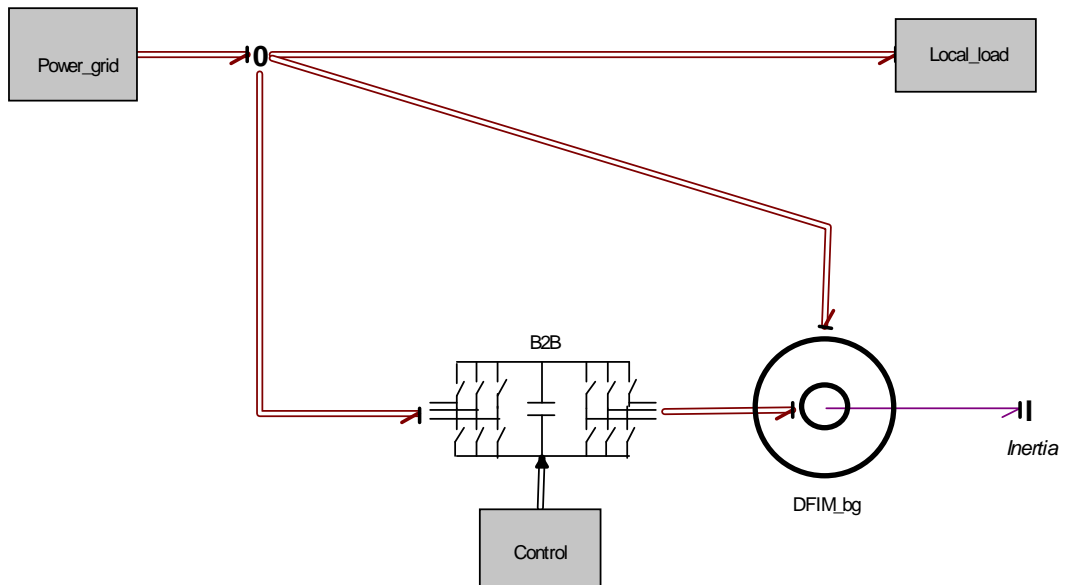
Figure 1: System overview.
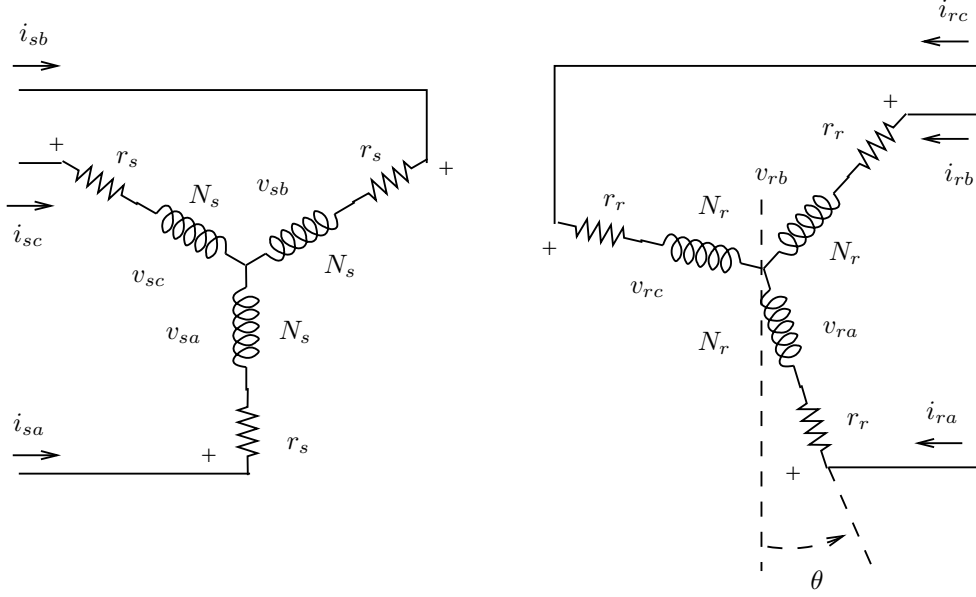

Figure 2: System overview in bond graph notation.

Figure 3: Basic scheme of the doubly fed induction machine

- stator-rotor cross inductances are smooth, sinusoidal functions of θ, with just the fundamental term.

To simplify the notation, we take $N_r = N_s = N$, so that we do not have to refer rotor variables to stator windings. Then

$$\tilde{L}(\theta) = \begin{pmatrix} \tilde{L}_s & \tilde{L}_{sr}(\theta) \\ \tilde{L}_{sr}^T(\theta) & \tilde{L}_r \end{pmatrix}$$

$$\tilde{L}_s = \begin{pmatrix} L_{ls} + L_{ms} & -\frac{1}{2}L_{ms} & -\frac{1}{2}L_{ms} \\ -\frac{1}{2}L_{ms} & L_{ls} + L_{ms} & -\frac{1}{2}L_{ms} \\ -\frac{1}{2}L_{ms} & -\frac{1}{2}L_{ms} & L_{ls} + L_{ms} \end{pmatrix} \quad \tilde{L}_r = \begin{pmatrix} L_{lr} + L_{mr} & -\frac{1}{2}L_{mr} & -\frac{1}{2}L_{mr} \\ -\frac{1}{2}L_{mr} & L_{lr} + L_{mr} & -\frac{1}{2}L_{mr} \\ -\frac{1}{2}L_{mr} & -\frac{1}{2}L_{mr} & L_{lr} + L_{mr} \end{pmatrix}.$$

Here L_{ls} and L_{lr} are leakage terms, while L_{ms} and L_{mr} are magnetizing terms that can be computed from the core reluctance $\mathcal{R}_m$ as

$$L_{ms} = L_{mr} = \frac{N^2}{\mathcal{R}_m}.$$

The cross-inductance is

$$\tilde{L}_{sr}(\theta) = L_{sr} \begin{pmatrix} \cos\theta & \cos(\theta + \frac{2}{3}\pi) & \cos(\theta - \frac{2}{3}\pi) \\ \cos(\theta - \frac{2}{3}\pi) & \cos\theta & \cos(\theta + \frac{2}{3}\pi) \\ \cos(\theta + \frac{2}{3}\pi) & \cos(\theta - \frac{2}{3}\pi) & \cos\theta \end{pmatrix}$$

where again $L_{sr} = \frac{N^2}{\mathcal{R}_m} = L_{ms}$. Hence (1) is a highly nonlinear set of ODE.

For a 2-pole machine, the torque is given in terms of the coenergy by

$$T_e(i, \theta) = \frac{\partial W_c(i, \theta)}{\partial \theta}$$

and since we are assuming a linear magnetic system, energy and coenergy are equal: $W_c = W_f = \frac{1}{2}i^T \hat{L}(\theta)i$.

Before proceeding to a θ-and-time-dependent transformation which eliminates most of the nonlinearities in (1), it is better to perform a constant transformation which reduces an effective degree of freedom for both the stator and the rotor. From the original (i, λ, v) quantities we compute (i', λ', v') by means of

$$y' = Ay \qquad (3)$$

where y is any of i, λ, v and A is a 6 by 6 block-diagonal matrix

$$A = \begin{pmatrix} A_s & 0 \\ 0 & A_r \end{pmatrix}$$

where

$$A_s = A_r = \begin{pmatrix} \frac{\sqrt{2}}{\sqrt{3}} & -\frac{1}{\sqrt{6}} & -\frac{1}{\sqrt{6}} \\ 0 & \frac{1}{\sqrt{2}} & -\frac{1}{\sqrt{2}} \\ \frac{1}{\sqrt{3}} & \frac{1}{\sqrt{3}} & \frac{1}{\sqrt{3}} \end{pmatrix}.$$

Notice that, since $A^T = A^{-1}$, this is a power-preserving transformation:

$$\langle i', v' \rangle = \langle i, v \rangle.$$

The components of y' are usually denoted by $y' = (y_d, y_q, y_0)$.
Under this transformation, relation (2) becomes

$$\lambda' = L'(\theta)i'$$

where

$$L'(\theta) = \begin{pmatrix} L_{ss} & 0 & 0 & M\cos\theta & -M\sin\theta & 0 \\ 0 & L_{ss} & 0 & M\sin\theta & M\cos\theta & 0 \\ 0 & 0 & L_{ls} & 0 & 0 & 0 \\ M\cos\theta & M\sin\theta & 0 & L_{rr} & 0 & 0 \\ -M\sin\theta & M\cos\theta & 0 & 0 & L_{rr} & 0 \\ 0 & 0 & 0 & 0 & 0 & L_{lr} \end{pmatrix} = \begin{pmatrix} L'_s & L'^T_m(\theta) \\ L'_m(\theta) & L'_r \end{pmatrix}$$

and $M = \frac{3}{2}L_{ms}$, $L_{ss} = L_{ls} + M$, $L_{rr} = L_{lr} + M$.
In the new (prime) variables, equation (1) becomes

$$v' = \frac{\mathrm{d}}{\mathrm{d}t}(L'(\theta)i') + Ri'. \qquad (4)$$

It can be seen from the form of L' that the homopolar components y_0 decouple from the rest, yielding an independent linear dynamics, and from now on we will drop them from the computations, although we will keep the same notation:

$$v' = \frac{\mathrm{d}}{\mathrm{d}t}(L'(\theta)i') + Ri', \qquad (5)$$

where now everything is 4-dimensional.
One can try to eliminate the complicate, θ-dependent terms in (5) by means of a change of variables (Blondel-Park transformation). There is a whole family of transformations, depending on an arbitrary time-dependent parameter $x(t)$:

$$f'' = K(x, \theta)f'$$

with

$$K(x, \theta) = \begin{pmatrix} K_s(x) & 0 \\ 0 & K_r(x, \theta) \end{pmatrix}$$

and

$$K_s(x) \equiv e^{-Jx} = B(x), \quad K_r(x, \theta) \equiv e^{-J(x-\theta)} = B(x - \theta), \qquad (6)$$

4

where

$$B(z) = \begin{pmatrix} \cos z & \sin z \\ -\sin z & \cos z \end{pmatrix}, \tag{7}$$

and

$$J = \begin{pmatrix} 0 & -1 \\ 1 & 0 \end{pmatrix}. \tag{8}$$

Notice that both K_s and K_r belong to SO(2) and hence this second transformation is also power preserving.

Under this transformation (5) becomes

$$v'' = \omega K(\partial_\theta L' - L'K^{-1}\partial_\theta K)K^{-1}i'' - \dot{x}KL'K^{-1}\partial_x KK^{-1}i'' + KL'K^{-1}\frac{\mathrm{d}i''}{\mathrm{d}t} + Ri'' \tag{9}$$

where $[K, R] = 0$ has been used. Taking into account that $B(x+y) = B(x)B(y)$ and $B(-x) = B^{-1}(x)$ and using (6), one gets

$$L'' \equiv KL'K^{-1} = \begin{pmatrix} L_{ss}\mathbb{I} & M\mathbb{I} \\ M\mathbb{I} & L_{rr}\mathbb{I} \end{pmatrix}. \tag{10}$$

Exploiting the fact that this L'' is independent of both x and θ, it is easy to derive the identities

$$\begin{aligned} KL'K^{-1}\partial_x KK^{-1} &= \partial_x KL'K^{-1}, \\ K(\partial_\theta L' - L'K^{-1}\partial_\theta K)K^{-1} &= -\partial_\theta KL'K^{-1}, \end{aligned}$$

whereupon (9) becomes

$$v'' = L''\frac{\mathrm{d}i''}{\mathrm{d}t} + \omega\Omega i'' + \dot{x}\Omega_x i'' + Ri'', \tag{11}$$

with

$$\Omega = -\partial_\theta KL'K^{-1} = \begin{pmatrix} 0 & 0 \\ -MJ & -L_{rr}J \end{pmatrix}, \tag{12}$$

$$\Omega_x = \partial_x KL'K^{-1} = \begin{pmatrix} L_{ss}J & MJ \\ MJ & L_{rr}J \end{pmatrix}. \tag{13}$$

The prize for a constant inductance matrix is a nonlinear term involving ω and i''. In what follows we will refer to the individual components of a f'' 4−vector as f_{sd}, f_{sq}, f_{rd}, and f_{rq}.

The co-energy in the transformed coordinates is given by

$$H_c(\theta, i) = \frac{1}{2}i^T L(\theta)i = \frac{1}{2}i''^T L''i'' + \text{homopolar contributions.}$$

However, the expression for the electrical torque T_e must be computed using the physical currents i. Hence

$$\begin{aligned} T_e &= \frac{1}{2}i^T\partial_\theta L(\theta)i \\ &= \frac{1}{2}i''^T KA\partial_\theta(A^T K^T L''KA)A^T K^T i'' \\ &= \frac{1}{2}i''^T K\partial_\theta(K^T L''K)K^T i'' \\ &= \frac{1}{2}i''^T L''\partial_\theta KK^T i'' + \text{transpose} \\ &= i''^T \mathcal{T}i'', \end{aligned} \tag{14}$$

where

$$\mathcal{T} = \begin{pmatrix} 0 & \frac{M}{2}J \\ -\frac{M}{2}J & 0 \end{pmatrix}. \tag{15}$$

The mechanical equation is (the mechanical part is transformation-independent)

$$J\ddot{\theta} = T_e - B\dot{\theta} + T_m$$

where J is the total inertia moment of the rotor, B is a friction coefficient and (T_m, ω) is the mechanical port to which any flywheel or rotating machinery can be coupled . Taking into account the form of T_e, this can be written as

$$\dot{\theta} = \omega \tag{16}$$
$$J\dot{\omega} = i''^T T i'' - B\omega + T_m. \tag{17}$$

The explicit PCH form is given by

$$\dot{z} = (\mathcal{J}(z) - \mathcal{R}(z))(\nabla H(z))^T + g(z)u,$$

where $z \in \mathbb{R}^n$, $\mathcal{J}$ is antisymmetric, $\mathcal{R}$ is symmetric and positive semi-definite and $u \in \mathbb{R}^m$ is the control. The function $H(z)$ is the hamiltonian, or energy, of the system. The natural outputs in this formulation are

$$y = g^T(z)(\nabla H(z))^T.$$

Equations (11) and (17) can be cast in this formulation with variables $z = (\lambda'', p = J\omega)$, hamiltonian function

$$H = \frac{1}{2}(\lambda'')^T (L'')^{-1} \lambda'' + \frac{1}{2J} p^2, \tag{18}$$

structure matrix

$$\mathcal{J} = \begin{bmatrix} -\dot{x}L_{ss}J & -\dot{x}M & O_{2\times 1} \\ -\dot{x}MJ & -(\dot{x}-\omega)L_{rr}J & MJi''_s \\ O_{1\times 2} & Mi''^T_s J & 0 \end{bmatrix}, \tag{19}$$

and dissipation matrix

$$\mathcal{R} = \begin{bmatrix} R_s I_2 & O_2 & O_{2\times 1} \\ O_2 & R_r I_2 & O_{2\times 1} \\ O_{1\times 2} & O_{1\times 2} & B_r \end{bmatrix}, \tag{20}$$

while the coupling is given by $g = I_5$ with the controls $u = (v''_{sd}, v''_{sq}, v''_{rd}, v''_{rq}, T_m)$. The bond graph corresponding to this description in the synchronous frame ($\dot{x} = \omega_s$) is shown in Figure 4. The stator and rotor resistances can be varied arbitrarily to include the effects of temperature. This dq model is embedded into a 3-phase model which includes the A and K transformations, as shown in 5.

1.3   The back-to-back converter

The iconic diagram for our three-phase converter appears in Figure 6.

The B2B is a Variable Structure System (VSS) which takes its power from the grid and delivers it in appropriate form to the rotor of the DFIM. Its control is implemented by 6 pairs (3 phases × 2 sides) of complementary switches. The main modelling challenge of this subsystem is the detailed description of the switches. For the model in Figure 6, we have used one of the possibilities offered by `20sim`, a variable-resistance implementation. The modularity of the approach allows for the replacement of this model by any other (the "hard model" [6], the averaged model [5], or the fixed causality model [7], for instance).

The whole B2B system has also been described as a PCH system, using the ideas in [6], and, in its averaged form, using the bond-graph formalism.
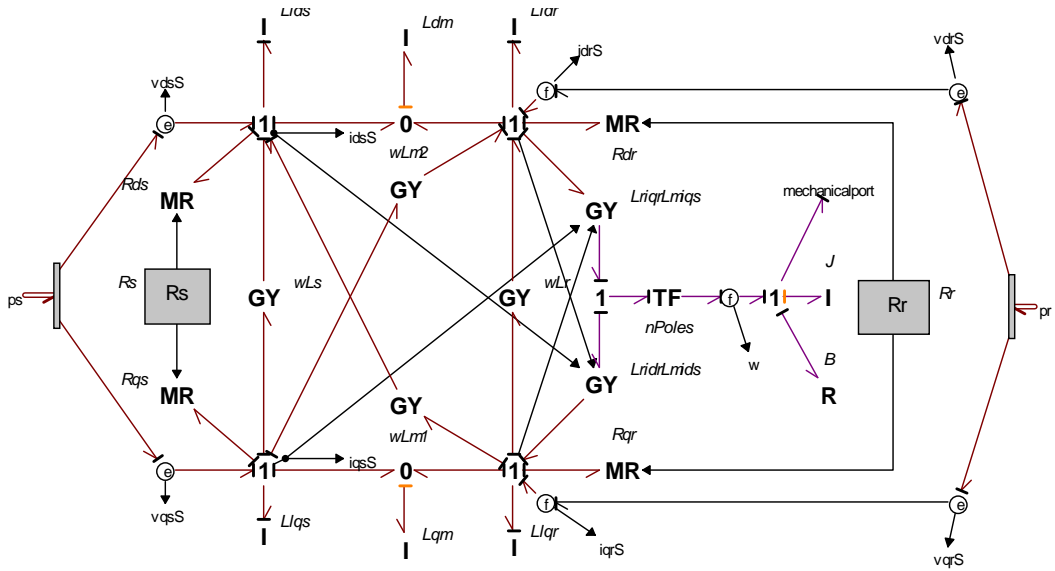
Figure 4: Bond graph of the DFIM in synchronous dq coordinates. The ω signal port is used to compute the rotor dq transformation.
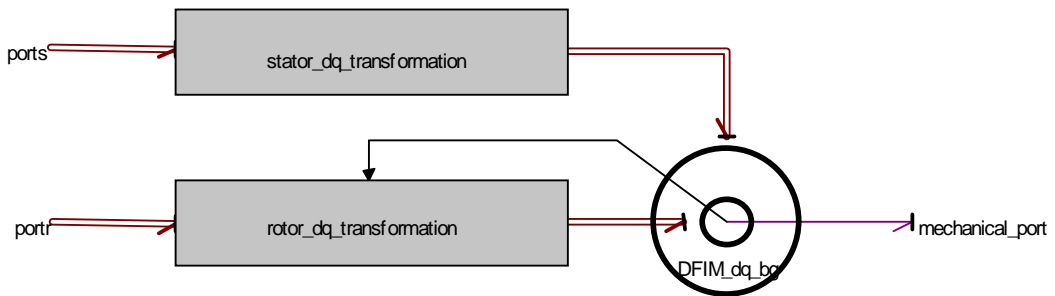

Figure 5: Bond graph of the 3-phase DFIM. It contains the dq power-preserving transformation and the DFIM dq model.
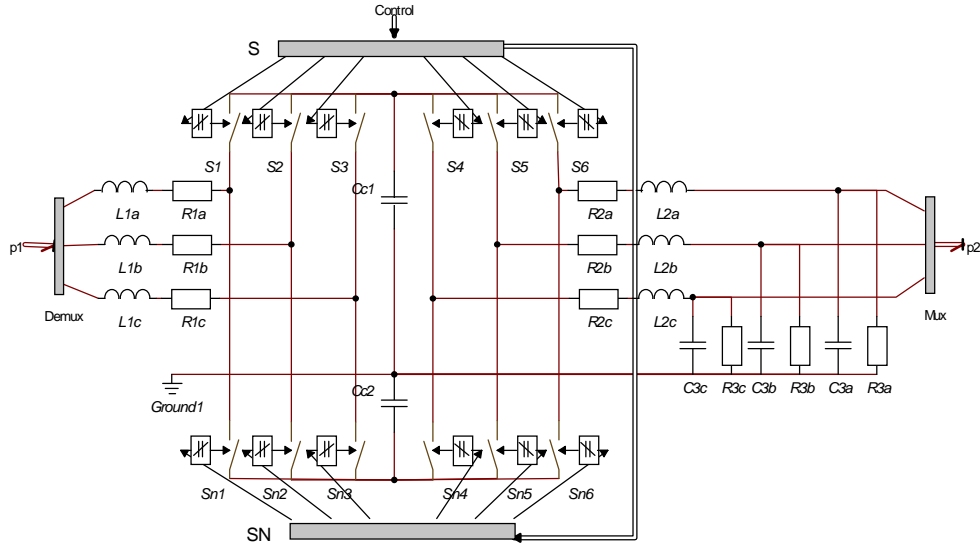
Figure 6: Iconic diagram of the back-to-back converter.

Overall connection	bond graph		
DFIM	PCH equations	bond graph	
B2B	"hard switch" PCH equations	iconic	bond graph averaged
Power grid	iconic	bond graph	
Local load	iconic	bond graph	
Local mechanical source	iconic	bond graph	

Table 1: List of submodels and port-based descriptions implemented.

1.4 Power grid, local load and mechanical source

Figures 7 and 8 show the models of the power grid and the local load chosen for this benchmark. The power grid contains a single 3-phase source and a Π model of the line, while the load is just a resistive charge, but anything could be added, or any other port-based description (PCH, bond graph) could be used. The mechanical source is just an inertia, representing the flywheel. Once more, the modularity of the port-based description allows the replacement of this simple model by any other, no matter how complex as long as its interface is a (torque, angular velocity) power port.

1.5 Submodel catalogue

Table 1 contains a list of the submodels implemented in this electromechanical benchmark.

1.6 Simulations

To present a simulation of the complete system, we have replaced the B2B with a transformer, as shown in Figure 9. The rotor angular velocity is displayed in Figure 10, for $n = 0$ and $n = 0.1$, where n is the turns-ratio parameter of the transformer. $n = 0$ corresponds to zero output voltage, *i.e.* rotor windings shorted, and in this case the DFIM goes to its synchronous regime, as expected; for $n = 0.1$ one gets a periodic behavior.
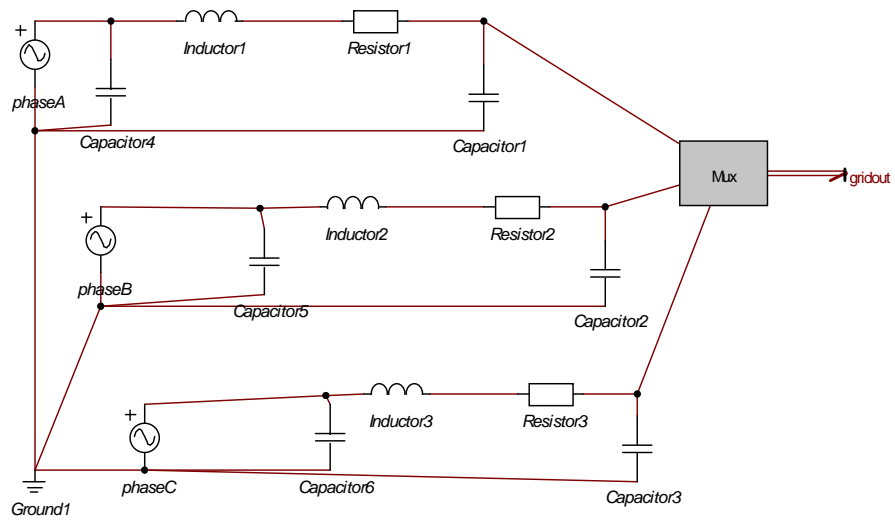
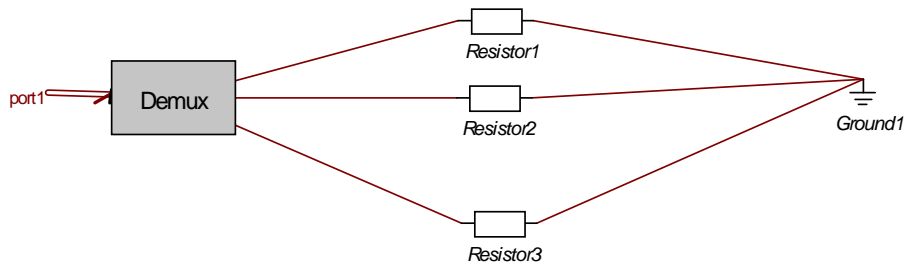Figure 7: Iconic diagram of a 3-phase Π model power line.

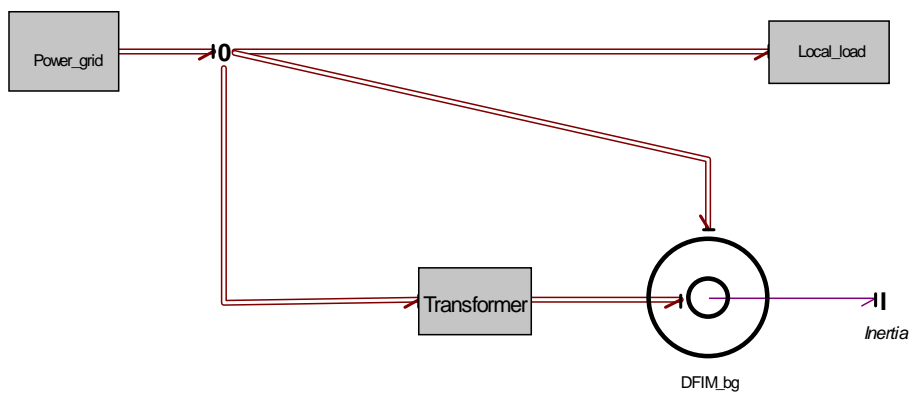Figure 8: Iconic diagram of a 3-phase resistive load.

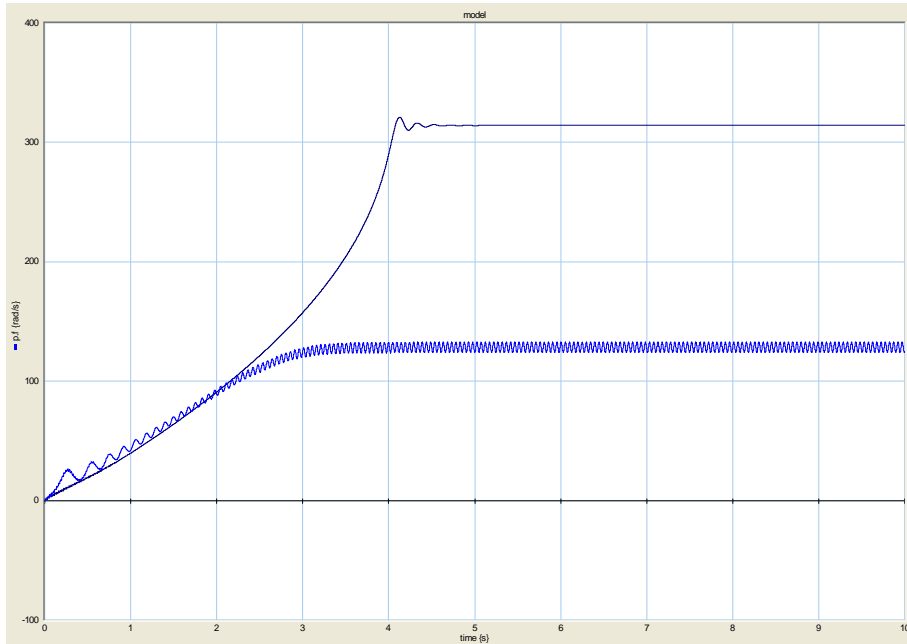Figure 9: Model used for simulations. A transformer has replaced the B2B.

Figure 10: Rotor angular velocity. For shorted rotor windings, it reaches the synchronous regime.

1.7   Control layer

As already explained, the detailed control is not a part of this benchmark. However, we will say a few words about it to show how everything will fit together.

The DFIM subsystem, together with a simplified version of the power grid and the load, can be controlled by means of IDA-PBC techniques [11] (see [3] for a technical discussion). Since we have not yet developed an IDA-PBC controller for the B2B implementing this DFIM controller, we have replaced the B2B by an ideal voltage source. This complete reduced system appears in Figure 11.

To test the control, the maximum power that the (ideal bus) power grid can provide is limited to 10 kW. At $t = 1$ the power needed by the local load starts to increase up to 30 kW, and the balance is provided by the energy stored in the flywheel. Shortly before $t = 2$ the power dissipated at the local load returns to its normal value, but the power taken from the grid is kept to its maximum for a while to return the flywheel to its near synchronous speed. The whole sequence is displayed in Figures 12 and 13.

1.8   Conclusions

This section describes some final remarks on port-based network modelling approach as applied to our electromechanical system.

1.8.1   Modularity

The port based concept allows the easy swapping of submodels and submodel descriptions. This is especially useful for testing controllers designed with parts of the submodels turned off or simplified to a large extent.
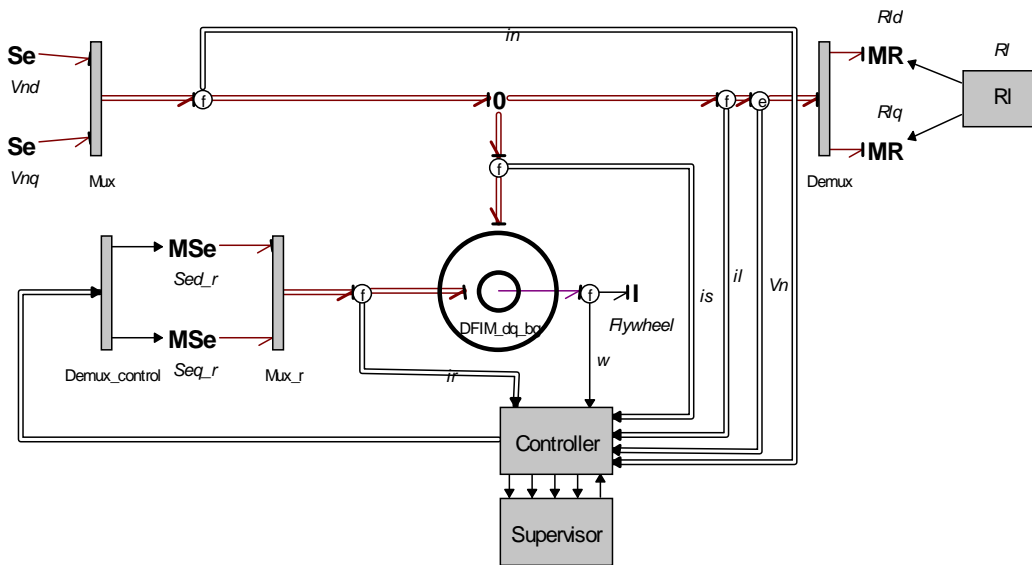
10

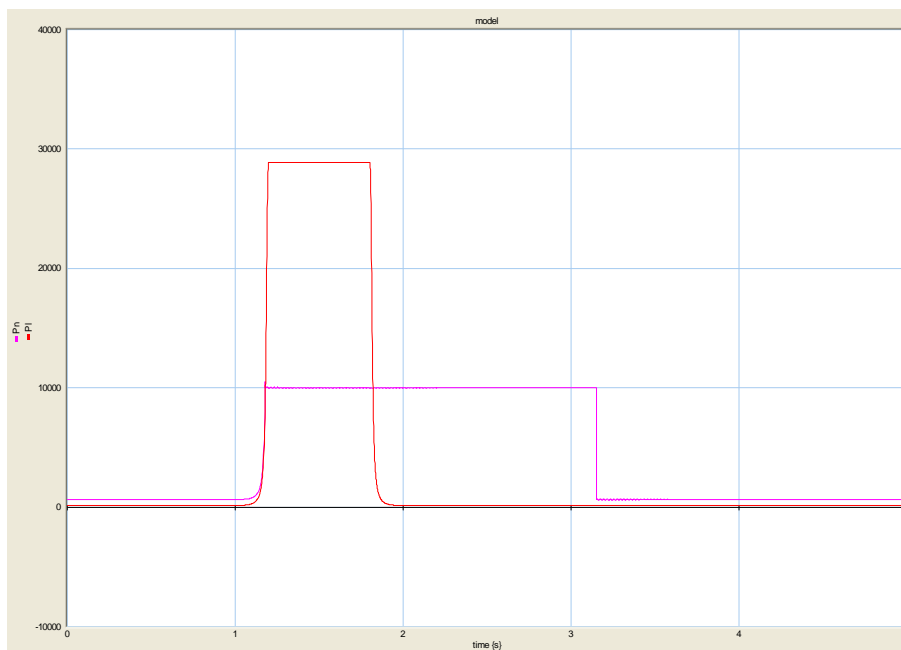Figure 11: Model used to test the control of the DFIM subsystem.

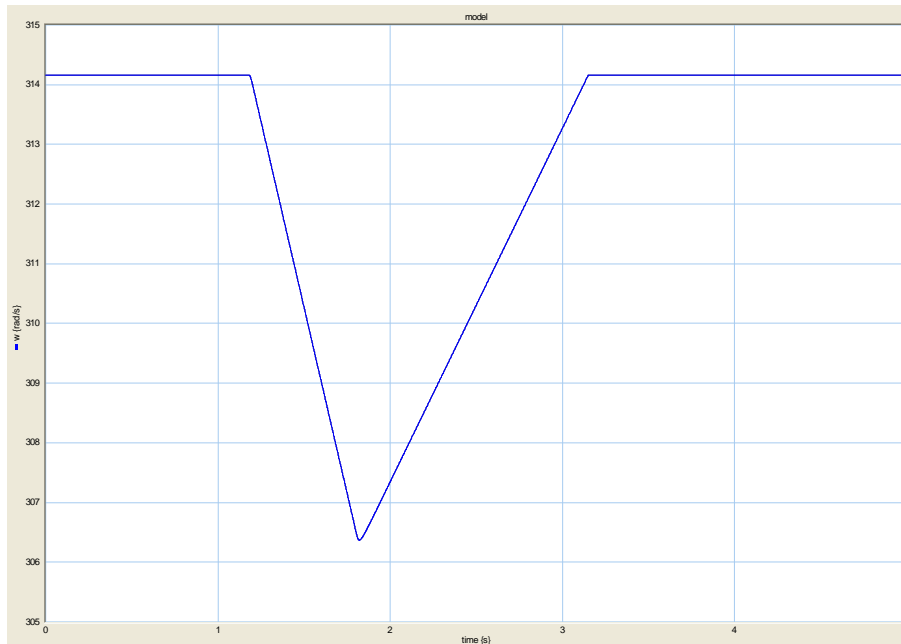Figure 12: Grid and load active powers.

Figure 13: Rotor angular speed.

1.8.2 Modelling issues

The electromechanical system that we have presented has two areas with room for modelling improvement.

1. **The variable structure of the B2B**. The "hard" description of the switches yields computational problems in the form of changing causalities. Two ways out of this is to use averaged models [1] or more complex descriptions of the switches with ancillary storage elements[7].

2. **The lumped parameter description of the DFIM**. In the present form, the DFIM cannot be decomposed as the interconnection of simpler elements since the electromagnetic field has been "integrated out" and its effect condensed into the mutual inductances between the different windings. A more fundamental description will have to use the distributed PCH formalism and its discretization proposed by several members of the Geoplex consortium or the distributed bond graph formalism and its Galerkin truncations [9].

References

[1] C. Batlle, D. Biel, E. Fossas, C. Gaviria, R. Griñó, and S. Martínez. GSSA and VSS models, Geoplex Deliverable D 4.1.1. Technical report, Geoplex consortium, 2003.

[2] C. Batlle, A. Dòria, E. Fossas, R. Griñó, and J. Riera. Tracking dynamics of the doubly fed induction machine. Technical report, UPC preprint, in preparation.

[3] C. Batlle, A. Dòria, and R. Ortega. Hamiltonian passivity-based control of a doubly-fed induction machine coupled to a flywheel. Technical report, SUPELEC and UPC preprint, in preparation.

[4] P. Breedveld. A generic dynamic model of multiphase electromechanical transduction in rotating machinery. In *Proceedings WESIC 2001*, pages 381–394. University of Tweente, June 27-29 2001.

[5] M. Delgado and H. Sira-Ramírez. Modeling and simulation of switch regulated dc-to-dc power converters of the boost type. *Proc. of the First IEEE International Caracas Conference on Devices, Circuits and Systems*, pages 84–88, 1995.

[6] G. Escobar, A. van der Schaft, and R. Ortega. A hamiltonian viewpoint in the modeling of switching power converters. *Automatica*, 35:445–452, 1999.

[7] P. H. Gawthrop. Hybrid bond graphs using switched i and c components. Technical Report CSC 97005, Centre for Systems and Control, University of Glasgow, 1997.

[8] P. C. Krause and O. Wasynczuk. *Electromechanical Motion Devices*. McGraw-Hill, 1989.

[9] F.-S. Lee. *Reticulation of distributed electromagnetic and electromechanical systems using the extended bond graph method*. PhD thesis, The University of Texas at Austin, May 1993.

[10] S. E. Lyshevski. *Electromechanical systems, electric machines and applied mechatronics*. CRC Press LLC, 2000.

[11] R. Ortega, A. van der Schaft, B. Maschke, and G. Escobar. Interconnection and damping assignment passivity-based control of port-controlled hamiltonian systems. *Automatica*, 38:585–596, 2002.